On the effect of nonuniform seeding on particle dispersion in two-dimensional mixing layers

Qunzhen Wang
Analytical Services & Materials, 244 East Avenue K-4, Lancaster, California 93534

Kyle D. Squires
Department of Mechanical and Aerospace Engineering, Arizona State University, Box 876106, Tempe, Arizona 85287-6106

Lian-Ping Wang
Department of Mechanical Engineering, University of Delaware, Newark, Delaware 19716

(Received 17 November 1995; accepted 16 March 1998)

The effect of nonuniform seeding on the dispersion of fluid elements and heavy particles has been investigated in two-dimensional, incompressible mixing layers. The cross-stream dispersion of fluid elements can be enhanced using nonuniform seeding with most particles near the saddle point because of the greater lateral extent of streamlines in this region, though the increase in dispersion compared to a uniform seeding occurs only after a few vortex turnover times. Compared to fluid elements, additional mechanisms—ejection from vortex cores, separatrix crossing, and the effect of the initial particle velocity—must be considered in the analysis of nonuniform seeding on heavy particle dispersion. The influences of these additional mechanisms are first investigated in a Stuart vortex. With increasing response time, vortex ejection and separatrix crossing shift the streamwise position maximizing lateral transport towards the vortex core. While changes in the initial particle velocity increase/decrease displacement, lateral dispersion may still be enhanced by appropriate nonuniform seeding of particles near the saddle point. Numerical simulations of the incompressible Navier–Stokes equations are then used to study cross-stream dispersion in a temporally evolving two-dimensional mixing layer. Stokes numbers St in the calculations were 0.05, 1, 10, and 100 where St is defined as the ratio of the particle response time to the time scale formed using the vorticity thickness of the initial mean flow. Particles were initially distributed nonuniformly at the interface between the two streams or along a line parallel to the interface. Simulation results show that the seeding location maximizing lateral dispersion is both time and Stokes number dependent, with larger increases in dispersion for the interface seeding. For Stokes numbers of order unity cross-stream dispersion exhibits a weak dependence on initial position since particles are efficiently ejected from the vortex core with subsequent motion confined to the nearby region outside the separatrix in one of the freestreams. Simulation results also show that substantial increases in particle dispersion can be obtained using nonuniform seedings relative to that obtained from an initially uniform distribution. © *1998 American Institute of Physics.* [S1070-6631(98)01407-X]

I. INTRODUCTION

Gas-phase turbulent free shear flows laden with small solid particles or liquid droplets are encountered in a wide variety of processes. Industrially relevant examples include the dispersion of liquid fuel droplets in combustors, coal particles in power plants, and aerosols in ventilation systems. In these and other applications it is the mixing of particles with the gas phase that often dictates the efficiency and stability of particular processes, e.g., droplet vaporization and mixing or contaminant removal. Thus, the ability to predict, and control, dispersion in free shear flows is important.

Of particular interest in this work is particle dispersion in a mixing layer. As is now well known, experimental and numerical results have demonstrated the existence of large scale coherent vortical structures in free shear flows. These structures, which originate from the roll up of the vorticity at the most unstable wavelength and pairing due to perturbations at subharmonic wavelengths, strongly influence both flow field dynamics as well as mixing processes (e.g., see Brown and Roshko,[1] Winant and Browand,[2] Ho and Huerre,[3] and Lazaro and Lasheras[4,5]). Particle dispersion in mixing layers and the effect of large scale structures have also been the subject of numerous studies (see Crowe *et al.*,[6] Chein and Chung,[7] Samimy and Lele,[8] Lazaro and Lasheras,[4,5] Hishida *et al.*,[9] Wen *et al.*,[10] Martin and Meiburg,[11] and Raju and Meiburg[12]). Both experimental and numerical studies indicate that the effect of the large scale structures on particle dispersion can be well characterized in terms of the particle Stokes number, St, which is defined as the ratio of the particle aerodynamic response time to the time scale of the large scale fluid motion (Crowe *et al.*[13–15]). Particles with small Stokes numbers follow the flow and have approximately the same dispersion as the fluid. Particles with large Stokes numbers are relatively unaffected by the flow since their response

time is substantially larger than the time scale of the large scale structures. Consequently, the dispersion of particles with large Stokes numbers is smaller than that of fluid elements. For intermediate Stokes numbers, e.g., of order one, particle dispersion can be substantially larger compared to fluid elements. The increased dispersion results from the fact that these particles can be flung from the core region of vortices (e.g., see Crowe *et al.*[13–15]).

Common to nearly all previous studies, both experimental and numerical, is that particle distributions were initially uniform. Wang[16] found that the stretching rate at the interface of a two-dimensional mixing layer varies relative to the vortex structure and proposed that a nonuniform initial distribution at the interface can alter the dispersion of fluid elements at later times. Wang[16] demonstrated that transverse dispersion of fluid elements, i.e., along the direction of the mean-velocity gradient, could be substantially increased or decreased by changing the initial seeding along the interface. A related work is that of Martin and Meiburg[11] where finite-inertia particles were initially seeded uniformly throughout one side of the mixing layer. Martin and Meiburg[11] found that particles crossing the interface ''*originate in fairly thick and slightly curved bands that emanate from the free-stagnation point,*'' implying a phase-coupled injection can enhance dispersion.

For fluid elements, nonuniform seedings with the largest fraction of particles near the saddle point significantly enhances cross-stream dispersion since the lateral extent of streamlines in this region are larger than at other locations in the layer (see Sec. II A). The rapid straining near the saddle also enhances mixing as discussed in Wang.[16] This larger straining and displacement of streamlines will affect the transport and mixing of finite-inertia particles (Martin and Meiburg[11]) and is expected to dominate for small inertia particles which follow similar paths as the fluid. However, as will be shown in this paper, the relative significance of this effect on dispersion control by nonuniform seeding is reduced as the particle response time is increased. There are at least three new mechanisms that arise for finite-inertia particles and must be considered. First, particle inertia results in the ejection of particles from the vortex core due to the large centrifugal force, which introduces a competing effect and favors a large seeding near the core of the vortex where the ejection rate is the largest. For small Stokes numbers, asymptotic analyses show that the effect of inertial bias on particle motion increases with St (Maxey[17]), implying that the fraction of particles seeded near the vortex center should increase with Stokes number in order to enhance dispersion.

Second, the ejection from vortex cores due to particle inertia induces a radial particle velocity, which will lead particles to cross over the separatrices, i.e., the streamlines passing through the saddle points. The separatrices divide the vortex core region from the free stream and play a significant role in the mixing process of fluid elements (Wang and Maxey[18]). In a steady flow, e.g., a Stuart vortex, fluid elements initially seeded at the interface will remain inside the vortex core bounded by the separatrices, while finite-inertia particles will cross over the separatrices and are left in the freestream at later times (see Sec. II B). This results in a very different dispersion pattern and a larger lateral transport compared to fluid elements. For two-dimensional temporally evolving mixing layers, even fluid elements initially at the interface can cross over the separatrices, leading to rapid mixing (Wang and Maxey[18]). It is expected that particle inertia will enhance the process of separatrix crossing in two ways. The first is that inertia will cause particles to cross the separatrices in a shorter time relative to fluid elements. In addition, while a significant fraction of fluid elements may be re-entrained into the vortex core in an unsteady mixing layer, finite-inertia particles are more likely to stay in the freestream once they have crossed through the separatrices. It should be noted that this enhanced separatrix crossing is closely related to the ejection mechanism. As a result, particles with Stokes numbers of order unity will be most efficiently removed from the vortex core and ejected into the freestream, leading to a weaker dependence of long-time lateral dispersion on the initial location. Therefore, the influence of separatrix crossings should reduce the effectiveness of nonuniform seeding on dispersion control. The fact that the underlying flow fields (streamline pattern and vorticity magnitude) inside and outside the vortex cores are significantly different makes the separatrix crossing an important event in the particle transport process. For this reason, the timing and persistence of separatrix crossings are worth considering on their own.

Finally, another complication relevant to considerations of nonuniform seeding for finite-inertia particles and not relevant to fluid elements, is that of initial conditions, i.e., the initial particle velocity. For increasing Stokes number the influence of the initial particle velocity becomes increasingly strong. In both the Stuart vortex and the unsteady mixing layer, the initial vertical fluid velocity along the interface varies with position, with a maximum occurring near the midpoint between the saddle and the vortex center. The maximum value in the mixing layer, of course, depends on the perturbation magnitude of the instability modes. The degree to which the initial particle velocity will affect dispersion depends on particle inertia and time. For finite-inertia particles, initial conditions can alter the effectiveness of dispersion control by nonuniform seeding.

The additional effects outlined above affecting the transport of finite-inertia particles, i.e., centrifuging from vortex cores, separatrix crossings, and initial conditions, are themselves connected to the underlying structure of the layer and a systematic examination of their effect on dispersion enhancement by nonuniform seeding has not been undertaken. While it would be advantageous to develop a theoretically based description of the effect of nonuniform seeding on the dispersion of finite-inertia particles, the coupled influences render the problem complex enough that analysis of a simplified flow is warranted.

Therefore, the primary objective of this work is to examine the effect of nonuniform seeding on particle transport in mixing layers. A complicating feature is their temporal and spatial development. The influences relevant to finite-inertia particles—lateral extent of streamlines, ejection from vortex cores, separatrix crossing, and initial conditions—can be more clearly studied through the examination of particle

motion in a simplified steady flow; in particular, a Stuart vortex. As shown in Sec. II, nonuniform seeding in a Stuart vortex enhances lateral transport and all the effects outlined above can be clearly observed. Numerical simulations of a two-dimensional mixing layer are then used to further corroborate the effectiveness of nonuniform seeding on particle dispersion for a range of Stokes numbers and to quantify increases in lateral transport. Unlike the previous results by Wang[16] and Martin and Meiburg,[11] which imply that a large seeding near the saddle point can enhance particle dispersion, it is shown in this work that the optimal seeding location depends on Stokes number and time, among other factors. The general conclusion is that for fluid elements the optimal seeding location is near the saddle point, for particles with $St=1$ nonuniform seeding has little effect on the long-time dispersion, for particles with larger St, the optimal location shifts towards the vortex center.

Finally, it should be remarked that in spatially developing mixing layers the method of nonuniformly seeding particles corresponds to a nonuniform injection in time [e.g., through an adjustment of the injection rate from the nozzle(s) used to seed particles]. Since nonuniform injection in applications can be performed (simultaneously) at various locations across the layer, it is also of interest to examine dispersion of particles seeded nonuniformly along a line away from the interface. Contained in Sec. II is an analysis of particle motion in a Stuart vortex, both for fluid elements (Sec. II A) and finite-inertia particles (Sec. II B). Following in Sec. III is a summary of the simulations of the temporally evolving mixing layer and processing of particle statistics. Calculations of particle dispersion using interface (Sec. IV A) and off-interface (Sec. IV B) seedings in a temporally evolving two-dimensional mixing layer then follow in Sec. IV. The main conclusions of the work are summarized in Sec. V.

II. PARTICLE TRANSPORT IN A STUART VORTEX

A. Fluid elements

In this section the transverse dispersion of particles seeded along the interface of a Stuart vortex is considered. The Stuart vortex is a steady flow which is an exact solution of the Euler equations. The stream function is

$$\psi(x,y)=\frac{\lambda\Delta U}{4\pi}\ln\left\{\cosh\left[\frac{2\pi y}{\lambda}\right]-\rho\cos\left[\frac{2\pi(x-0.5\lambda)}{\lambda}\right]\right\}, \tag{1}$$

where ΔU is the velocity difference across the layer and λ the wavelength. Note that this form of the Stuart vortex has saddle points at $(x,\ y)=(n\lambda,\ 0)$ and vortex center at $((0.5+n)\lambda,\ 0)$, where $n=0,\pm1,\pm2,\ldots$. The parameter ρ controls the shape of the vortex: $\rho=1$ corresponding to a periodic row of point vortices while $\rho=0$ to a parallel shear flow. The large scale vortical structures in a typical mixing layer are similar to the Stuart vortex with $\rho=0.25$ (Stuart,[19] Ho and Huerre,[3] and Meiburg and Newton[20]) and this value is used for the calculations presented in this section. The streamlines (1) are shown in Fig. 1(a), which indicates that the streamline passing through the saddle point (0, 0) has the largest semiheight H (defined as the y value of the intersection between the streamline and the line $x=0.5\lambda$) compared to other points along the interface. The semiheight of the streamline passing through the point $(x,\ 0)$ can be derived as

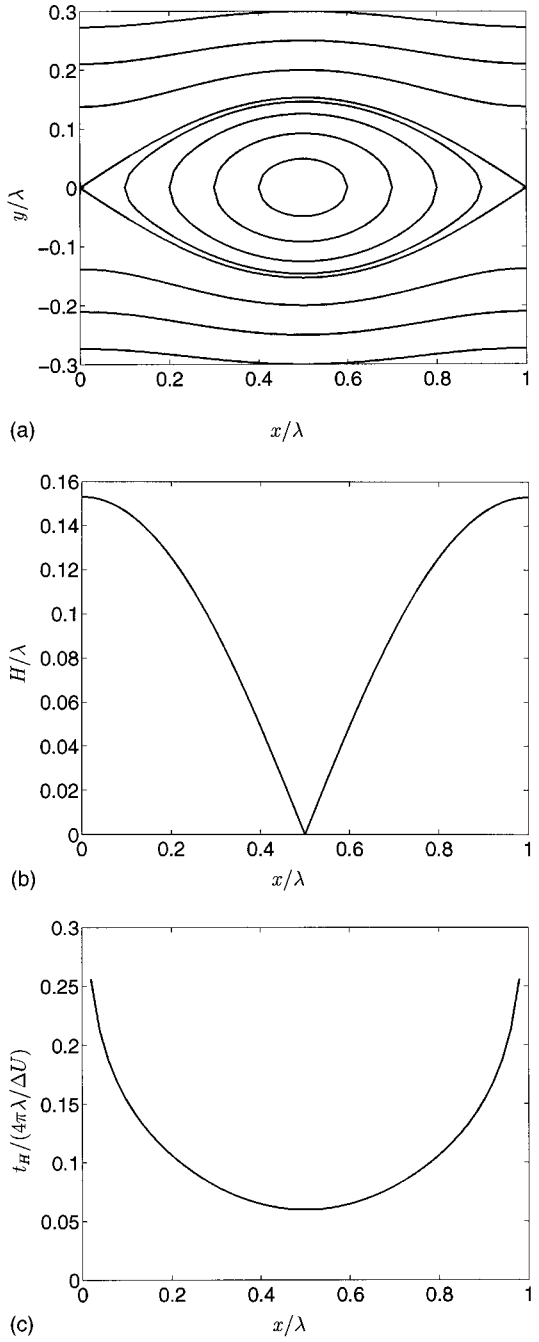

FIG. 1. Streamlines and semiheight H of the streamline passing through the point $(x,0)$ as well as the time needed for fluid elements to reach semiheight in the Stuart vortex. (a) Streamlines; (b) semiheight of the streamline passing through $(x,0)$; (c) the time required for fluid elements travel from $(x,0)$ to $(0.5,H)$.

$$H(x)=\frac{1}{2\pi}\cosh^{-1}\left\{1+\rho-\rho\ \cos\left[\frac{2\pi(x-0.5\lambda)}{\lambda}\right]\right\}, \tag{2}$$

which is shown in Fig. 1(b). The figure shows that the semiheight is maximum for the saddle points, zero for the vortex center, and takes on values $0<H/\lambda<0.153$ for the other points along the interface. Therefore, of the fluid elements

initially along the interface, those near the saddle point will have the largest lateral dispersion. Consequently, a nonuniform seeding with a larger fraction near the saddle will have larger transverse dispersion than can be achieved using a uniform seeding, as shown previously in the calculations by Wang.[16]

While Fig. 1(b) shows fluid particles initially seeded near the saddle points will have large lateral transport, an important consideration is the time t_H required for fluid elements to reach the semiheight H. Although the semiheight for the saddle point is the largest (cf. Fig. 1(b)), an infinite time $t_H \to \infty$ is required for particles to reach $(0.5\lambda, H)$ since the velocity vanishes there. Figure 1(c) shows t_H as a function of streamwise location along the interface. It is clear that t_H decreases dramatically for fluid elements further from the saddle point (i.e., closer to the vortex center). The important point illustrated by Fig. 1(c) is that the nonuniform seeding yielding the largest dispersion is time-dependent, e.g., fluid particles initially between the saddles and vortex center will have the largest lateral transport early in the evolution of the trajectories. Only at long times will a seeding with the largest fraction of fluid elements near (but not at) the saddle point yield the largest cross-stream dispersion.

B. Finite-inertia particles

Finite-inertia particles do not follow the same trajectories as fluid elements and therefore cross-stream dispersion might not be maximized using seedings with a larger fraction of particles near the saddle. To examine the additional effects described in the Introduction, particle trajectories are calculated for a range of Stokes numbers in which particle motion is described using a simplified form of the equation of motion derived by Maxey and Riley,[21]

$$\frac{dv_i}{dt} = -\frac{v_i - u_i}{\tau_p}, \tag{3}$$

where v_i is the velocity of the particle and u_i is the velocity of the fluid at the particle position. Equation (3) describes the motion of particles with densities substantially larger than that of the surrounding fluid and diameters small compared to the smallest scales of the flow. A linear (Stokes) drag law has been used which is applicable for small particle Reynolds numbers. The response time in (3) is $\tau_p = (2\rho_p a^2)/(9\rho_f \nu)$ where ρ_p and ρ_f are the densities of the particle and fluid, respectively, a is the particle radius, and ν is the fluid kinematic viscosity. Assuming that the terminal velocity of the particle is much less than the velocity scale in a mixing layer, we neglect the body force term in (3). It should also be noted that (3) neglects the influence of virtual mass, buoyancy, and the Basset history force on particle motion. For particles with material densities large compared to the fluid these forces are negligible compared to the drag.

Shown in Fig. 2 are trajectories of fluid elements and finite-inertia particles. For the finite-inertia particles, the initial velocity was set equal to the fluid velocity at the particle position. Trajectories for a range of initial positions along the interface and for a time interval corresponding to about one ''vortex turnover time'' $(t/(\lambda/\Delta U) = 0.9)$, are shown. The

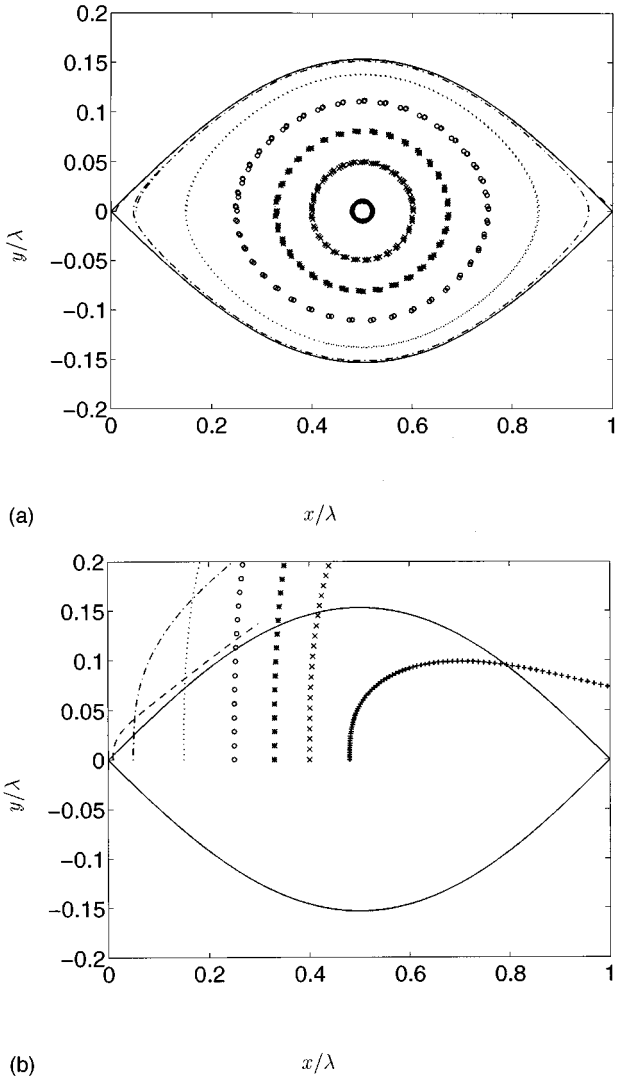

FIG. 2. Particle trajectories in the Stuart vortex, separatrix shown as a solid line. The time step $dt/(\lambda/\Delta U) = 0.0001$ and the total integration time $t/(\lambda/\Delta U) = 0.9$. (a) Fluid elements; (b) $\tau_p/(\lambda/\Delta U) = 1$. - - -, $x_0/\lambda = 0.01$; — - —, $x_0/\lambda = 0.05$; ⋯, $x_0/\lambda = 0.15$; ○, $x_0/\lambda = 0.25$; *, $x_0/\lambda = 0.33$; ×, $x_0/\lambda = 0.40$; +, $x_0/\lambda = 0.48$.

circulatory nature of the fluid particle trajectories in Fig. 2(a) is evident, with the lateral transport of particles seeded near the core remaining small. The separatrix has also been drawn and shows, as expected, that for initial seedings along the interface, there is no separatrix crossing by fluid elements. In Fig. 2(b), however, the inability of finite-inertia particles to follow similar trajectories as the fluid is also clear. Consequently, finite-inertia particles are ejected from the core region of the vortex and cross the separatrix relatively rapidly. Due to a rapid ejection into the freestream, nonuniform seeding will be a less effective means of controlling dispersion. In addition, while the cross-stream dispersion of fluid particles will be enhanced due to the larger lateral extent of streamlines emanating from the saddle point, a comparison of Fig. 2(a) and 2(b) indicates that the effect of particle ejection and separatrix crossing changes the optimal seeding location of finite-inertia particles compared to that for fluid elements.

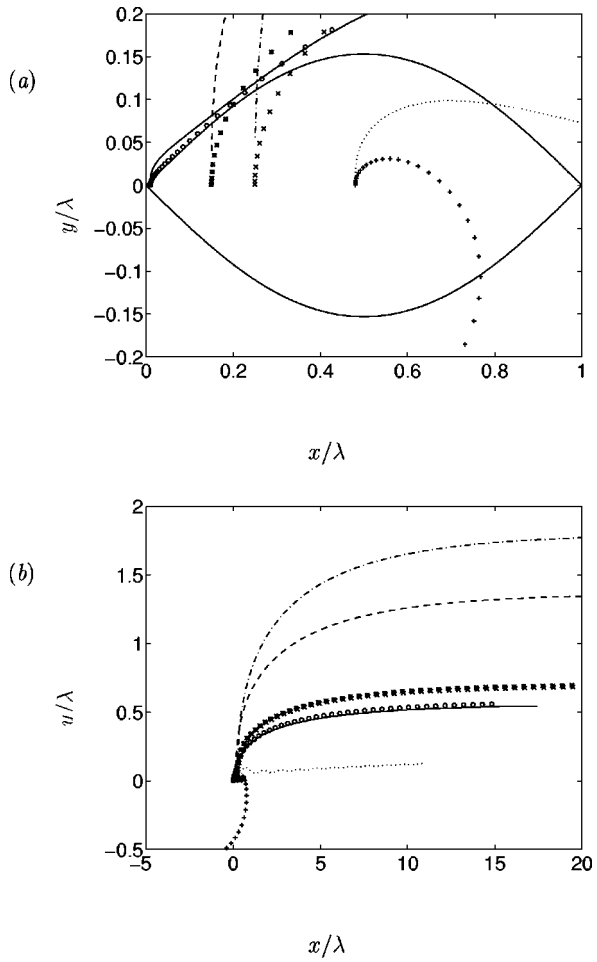

FIG. 3. Particle trajectories in the Stuart vortex; the separatrix shown as a solid line in (a). The time step $dt/(\lambda/\Delta U)=0.0001$. (a) $0\leqslant t/(\lambda/\Delta U)\leqslant 2.25$; (b) $0\leqslant t/(\lambda/\Delta U)\leqslant 4.5$. Initial particle velocity equal to fluid velocity at the particle position: ——, $x_0/\lambda=0.01$; ---, $x_0/\lambda=0.15$; — - —, $x_0/\lambda=0.25$; ···, $x_0/\lambda=0.48$; initial particle velocity equal to zero: ○, $x_0/\lambda=0.01$; *, $x_0/\lambda=0.15$; ×, $x_0/\lambda=0.25$; +, $x_0/\lambda=0.48$.

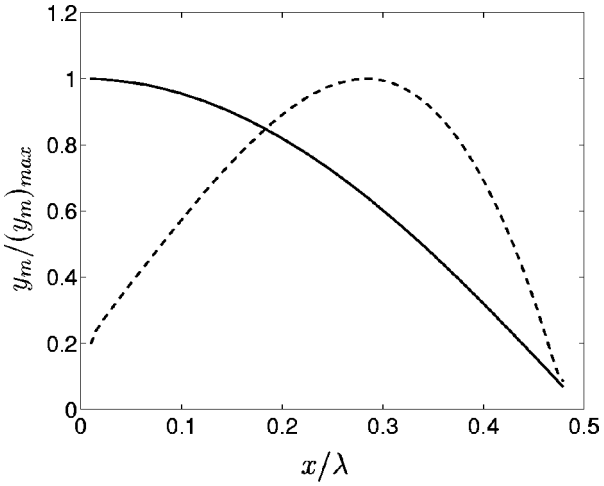

FIG. 4. Maximum cross-stream dispersion as a function of the initial streamwise location in the Stuart vortex. ——, fluid elements; ---, $\tau_p/\lambda/\Delta U=10$.

Shown in Fig. 3 are trajectories for the same initial conditions as considered in Fig. 2(b) as well as trajectories in which the initial particle velocity is zero. The short-time evolution in Fig. 3(a) again shows the separatrix crossings occurring as particles are ejected from the core region. For the initial particle velocities considered, i.e., zero or the value of the fluid velocity, there is a relatively minor effect on transport for particles seeded near the saddle ($x_0/\lambda=0.01$) because the fluid velocity is small in this region. As the fluid velocity increases away from the saddle, the effect of the initial particle velocity is more significant and there are larger differences evident in displacement in Fig. 2(a), with particles having initial velocity identical to the fluid seeded near or at the mid-point $x_0/\lambda=0.25$ crossing the separatrix earlier. The complex effect of the initial conditions is apparent for the trajectories from $x_0/\lambda=0.48$ where for an initial velocity of zero the particle crosses the lower separatrix, while for an initial velocity equal to that of the fluid the particle is ejected from the core over the upper separatrix.

Following the evolution in Fig. 3(a), the effect of the initial velocity on transport at longer times in Fig. 3(b) shows, in general, a larger lateral transport for particles with initial velocity equal to the fluid velocity. In particular, for initial seedings near or at $x_0/\lambda=0.25$, where the cross-stream fluid velocity is largest, the lateral transport differs by more than a factor of two for particles with initial velocities equal to the fluid compared to initial velocities equal to zero. The effect of initial conditions will become stronger for increasing particle inertia and this will in turn lead to larger differences in displacement for different initial conditions. While changes in the initial particle velocity will increase or decrease lateral transport, it is interesting to note that, unlike the dispersion of fluid elements which is maximized for initial seedings near the saddle, the cross-stream dispersion for finite-inertia particles is larger at points away from the saddle for both initial conditions.

It is also important to note that, while ejection, separatrix crossing, and initial conditions alter the dispersion of finite-inertia particles compared to fluid elements, Figs. 2 and 3 show lateral transport of finite-inertia particles remains sensitive to initial position and that nonuniform seeding may still be used to maximize cross-stream dispersion. To further illustrate this point, trajectories were calculated for a range of particle response times. A representative plot showing the maximum cross-stream dispersion as a function of initial streamwise location is shown in Fig. 4. The initial condition was that the particle velocity was equal to the fluid velocity. Note that Fig. 3(b) shows that after particles are ejected into the far-field freestream, the cross-stream dispersion becomes nearly independent of time. Thus, the ''maximum'' dispersion in Fig. 4 corresponds to the asymptotic limit in which there is virtually no change in lateral dispersion (integration times greater than $100\lambda/\Delta U$). For fluid elements, consistent with Fig. 1(b), the dispersion is largest for initial positions near the saddle $x=0$. The peak then moves towards the core for finite-inertia particles. The shift away from the saddle again illustrates the contribution of the additional effects relevant to finite-inertia particles (cf. Figs. 2–3). The increased semiheight of the streamline, which favors a greater seeding of particles near the saddle, is less effective for finite-inertia

particles due to vortex ejection by centrifugal forces, separatrix crossing, and initial conditions. Thus, while the transverse dispersion of fluid elements can be maximized (at long times) with the greatest fraction of particles seeded near the saddle, for particles with finite inertia the optimal seeding location is shifted to regions between the saddle and vortex center.

The above discussions using a steady Stuart vortex illustrate the various physical mechanisms affecting dispersion control of finite-inertia particles. Our main interest is to study how these mechanisms contribute to the effectiveness of dispersion control in an unsteady mixing layer. Described in the next section is an overview of the simulations; results from the calculations are then presented in Sec. IV.

III. SIMULATION OVERVIEW

A. Calculation of a temporally evolving mixing layer

The evolution of a two-dimensional mixing layer was calculated through numerical simulation of the incompressible Navier–Stokes equations using the fractional step method (e.g., see Kim and Moin,[22] Perot,[23] and Wu *et al.*[24]). Spatial derivatives are evaluated using second-order accurate central differences. The discretized system is time advanced using second-order Adams-Bashforth for the convective terms and the Crank-Nicholson method for the viscous terms. The Poisson equation for pressure was solved using Fourier series expansions in the streamwise direction together with tridiagonal matrix inversion (see Williams[25] and Kim and Moin[22]).

The initial mean velocity in the streamwise (x) direction was a hyperbolic-tangent profile,

$$u_0(y)=\tfrac{1}{2}\tanh y. \tag{4}$$

The profile (4) was perturbed using eigenfunctions obtained from linear stability analysis, i.e.,

$$u_1(x,y)=u_0(y)+A.\mathscr{R}\{\hat{u}_F(y)e^{i\alpha_F x}\}, \tag{5}$$

$$u_2(x,y)=A.\mathscr{R}\{\hat{v}_F(y)e^{i\alpha_F x}\}, \tag{6}$$

where $\hat{u}_F$ and $\hat{v}_F$ are the eigenfunction of the streamwise and cross-stream velocities of the fundamental mode. The most amplified two-dimensional wave for the incompressible flow with the mean profile (4) has a wavenumber $\alpha_F=0.4446$ (Michalke[26]), which corresponds to a wavelength,

$$\lambda=\frac{2\pi}{\alpha_F}=14.132. \tag{7}$$

Note that $\hat{u}_F$ and $\hat{v}_F$ in (5) and (6) are complex functions and $\mathcal{R}\{\hat{u}\}$ denotes the real part. The disturbance magnitude was chosen as $A=0.04$ for which the perturbation field is still in its stage of linear instability. Following Michalke,[26] eigenfunctions were normalized such that the real part of the eigenfunction at the interface ($y=0$) was unity.

The computational domain in the streamwise direction was chosen as $L_x=\lambda$ while in the cross-stream direction $L_y=5\lambda$. The reference Reynolds number $Re=\Delta U\delta_{\omega 0}/\nu$ was 1000 where δ_ω is the vorticity thickness,

$$\delta_\omega=\frac{\Delta U}{(\partial\overline{u_1}/\partial y)_{y=0}}, \tag{8}$$

and $\overline{u_1}$ is the mean streamwise velocity, $\delta_{\omega 0}$ is the value at $t=0$. The governing equations were resolved using 256×257 grid points with a uniform grid in the streamwise direction and a hyperbolic-tangent stretched grid in the cross-stream direction. Simulations conducted at a coarser resolution (128×129 grid points) were nearly identical to the fine-grid results. For the temporally-evolving layer periodic boundary conditions are appropriate for the streamwise direction. No-stress boundary conditions were applied in the cross-stream direction, i.e., $u_2=\partial u_1/\partial x_2=0$ where u_1 and u_2 are the streamwise and cross-stream velocity, respectively.

B. Particle statistics

Particle motion was calculated using (3). From computation of an Eulerian velocity field as described in Sec. III A, (3) was integrated in time using second-order Adams–Bashforth. The initial particle velocities were zero. Since it is only by chance that a particle is located at a grid point where the Eulerian velocity field is available, fourth-order Lagrange polynomials were used to interpolate the fluid velocity to the particle position (see Wang *et al.*[27] for a further discussion). Particle displacements were also integrated using the second-order Adams–Bashforth method. For particles that moved out of the domain in the streamwise direction periodic boundary conditions were used to reintroduce it in the computational domain. The extent of the domain in the cross-stream direction was large enough such that no particles moved laterally out of the computational box.

For the temporally evolving mixing layer particle Stokes numbers are defined as $St=\tau_p/\tau_f$, where τ_f is a time scale of the large eddies. This definition of St in terms of a large-eddy time scale is conventional for free shear flows (e.g., see Crowe *et al.*[13–15]). There is, however, a slight ambiguity in the choice of τ_f. In this section the flow time scale is defined using the initial vorticity thickness and velocity difference between the upper and lower streams, i.e., $\tau_f=\delta_{\omega 0}/\Delta U$. As shown in the following figures, this is an appropriate scaling for ''short-time'' dispersion, i.e., transport times on the order $\delta_{\omega 0}/\Delta U$. Nondimensionalization of the response time using $\lambda/\Delta U$, as employed in the previous section, is a better scaling for long-time dispersion ($\lambda/\delta_{\omega 0}=7.1$). It should also be noted that using the dominant frequency to define τ_f as suggested by Aggarwal,[28] i.e., $\tau_f=1/\alpha_F$, yields $\tau_f=2.25$, close to the value $\tau_f=\delta_{\omega 0}/\Delta U=2$.

The mean-square dispersion was obtained using 20,000 trajectories for each Stokes number $St=0.05$, 1, 10, and 100. Particles were initially seeded nonuniformly along the interface of the layer ($y_0=0$) (see Sec. IV A) or a line parallel to the interface representative of the location where both the freestream and roll up of the vortex influence dispersion ($y_0=0.1\lambda$) (see Sec. IV B). For the interface seeding $y_0=0$ the trajectories of 10,000 particles were obtained, initially seeded in the left half of the domain ($x<\lambda/2$) and symmetry conditions were used to obtain the trajectories of

the remaining 10,000 particles. For the off-interface seeding there is no symmetry and it is therefore necessary to explicitly calculate the trajectories of all 20,000 particles.

The primary measure used to quantify the effect of nonuniform seeding on transport is the mean-square dispersion in the cross-stream direction,

$$Y^2(t|y_0)=\langle y^2(t|x_0,y_0)\rangle, \tag{9}$$

where $y(t|x_0,y_0)$ is the location of the particle at time t whose initial location is (x_0,y_0). The angle brackets, $\langle\ \rangle$, denote the average over the initial particle distribution in the streamwise direction. The effect of nonuniform seeding is studied by varying this initial distribution function, $f(x_0)$. In terms of $f(x_0)$, (9) can be equivalently written as

$$Y^2(t|y_0)=\int_0^{L_x} y^2(t,x_0)f(x_0)dx_0. \tag{10}$$

Accurate estimation of the integral in (10) requires a proper discretization of x_0. In particular, the initial distribution of particles tracked in the simulations represents effectively the discretization method and is prescribed carefully to maintain small separations between any two neighboring particles throughout the calculation (e.g., see Wang[16]). It is important to point out that this initial distribution of the tracked particles required for accurate evaluation of (10) is a separate consideration from the functions used to achieve nonuniform seedings, which is completely controlled by $f(x_0)$. Equation (10) was discretized as

$$Y^2(t|y_0)=\sum_{k=1}^{M-1}\frac{y^2(t,x_0^k)+y^2(t,x_0^{k+1})}{2}\ f\left(\frac{x_0^k+x_0^{k+1}}{2}\right)\times(x_0^{k+1}-x_0^k), \tag{11}$$

where $M=20{,}000$ is the total number of particles and x_0^k is the initial location of the kth particle followed in the simulation.

The effect of nonuniformity in the initial seeding was examined using a distribution of the form

$$F(x_0)=\begin{cases}\dfrac{1}{\sqrt{2\pi}\sigma}\exp\left\{-\dfrac{(x_0-x_{m1})^2}{2\sigma^2\lambda^2}\right\}, & \text{for } 0\leqslant\dfrac{x_0}{\lambda}<0.5,\\[2ex] \dfrac{1}{\sqrt{2\pi}\sigma}\exp\left\{-\dfrac{(x_0-\lambda+x_{m2})^2}{2\sigma^2\lambda^2}\right\}, & \text{for } 0.5\leqslant x_0/\lambda\leqslant 1.0.\end{cases} \tag{12}$$

Note that this distribution corresponds to a relatively larger seeding of particles near $x_0=x_{m1}$ and $x_0=\lambda-x_{m2}$, where x_{m1} and x_{m2} are the distance from the peak of the distribution to the saddle points. For particles initially seeded along the interface we set $x_{m1}=x_{m2}=x_m$ because of symmetry. While x_{m1} and x_{m2} allow variation of the optimal seeding location and are determined by studying representative particle trajectories, the parameter σ controls the degree of nonuniformity of the initial distribution, i.e., smaller σ corresponding to greater nonuniformity. Therefore, the distribution (12) is rather general for the purpose of this study. The distribution function was normalized in order that $f(x_0)$ have unit area, i.e.,

$$f(x_0)=\frac{1}{\int_0^{L_x}F(x_0)dx_0}F(x_0). \tag{13}$$

IV. PARTICLE TRANSPORT IN A TEMPORALLY EVOLVING MIXING LAYER

A. Interface seeding

1. Particle trajectories

Prior to calculations used to quantify the effect of nonuniform seeding on dispersion using a large (20,000) ensemble, it is instructive to examine particle trajectories for a smaller sample size, similar to that used in the Stuart vortex in Sec. II. The main goal is to gain some insight into the differences in transport in the evolving (unsteady) flow compared to the steady Stuart vortex. In addition, the trajectories help determine the optimal seeding locations to be used in (12) for the subsequent calculations using a large ensemble of particles. Shown in Fig. 5 are trajectories from a representative range of initial positions along the interface for fluid elements and finite-inertia particles with $St=1$, 10, and 100. The time axis in the following figures has been made dimensionless using λ and ΔU, i.e., $T\equiv t/(\lambda/\Delta U)$. Note also that, due to symmetry, it is sufficient to consider trajectories for initial seedings $0<x_0/\lambda<0.5$. Separatrices have also been drawn for representative times at which some particles have crossed the separatrix. For the evolving mixing layer, the separatrix at any given time is defined as the enclosed, instantaneous streamline passing through the two fixed saddle points at $x=0$ and $x=\lambda$ with $y=0$. The fluid element trajectories in Fig. 5(a) are qualitatively similar to those for the Stuart vortex (cf. Fig. 2(a)). For the time interval shown ($T=2.8$) none of the fluid elements cross the separatrix and the largest lateral transport occurs slightly away from the saddle. This again illustrates the time-dependent nature of the dispersion, i.e., the larger cross-stream transport for fluid elements seeded near the saddle will occur at longer times than shown in Fig. 5(a). At longer transport times, some fluid elements will cross the separatrix and then be re-entrained. Cross-stream dispersion will also be maximized for particles initially seeded near the saddle.

The trajectories for $St=1$, 10, and 100 show similar effects as illustrated earlier in the Stuart vortex, in addition to other interesting features due to the time-dependent nature of the flow. For example, following the separatrix crossings, for $St=1$ the trajectories ''wobble'' in response to the quasi-periodic shrinking and expansions of the vortex core. It is also interesting to note that the trajectories become relatively independent of the initial position, implying that at ''long times,'' i.e., within about 5–6 turnover times, there is a weak dependence of dispersion on nonuniform seeding for $St=1$. This is consistent with the fact that for Stokes numbers of order unity, particles are efficiently removed from the core region, becoming relatively independent of their initial conditions.

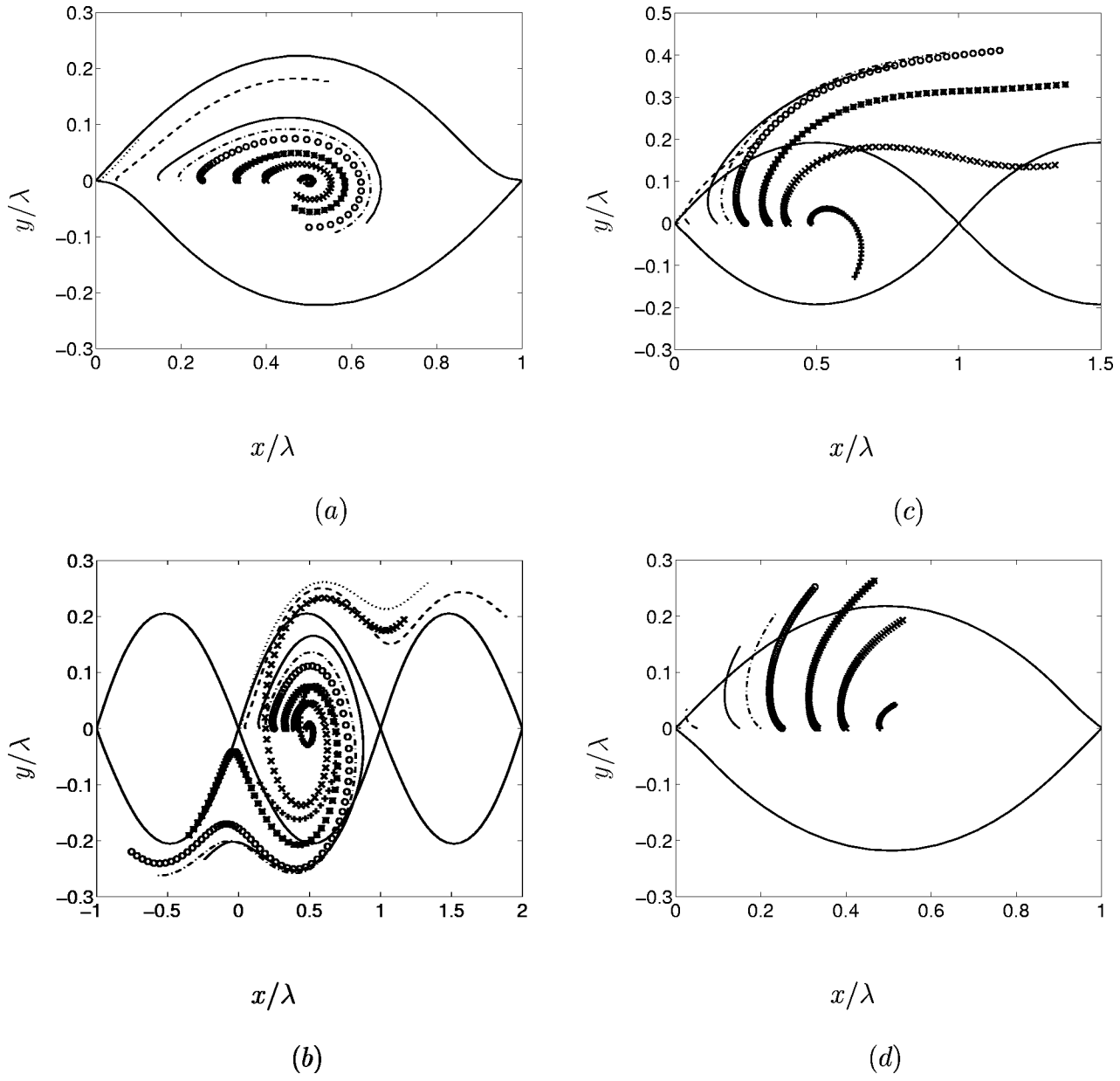

FIG. 5. Particle trajectories from initial locations along the layer interface. (a) Fluid elements at $0 \leqslant T \leqslant 2.8$; (b) $St=1$ at $0 \leqslant T \leqslant 6.4$; (c) $St=10$ at $0 \leqslant T \leqslant 5.7$; (d) $St=100$ at $0 \leqslant T \leqslant 7.1$. Initial streamwise location: ⋯, $x_0/\lambda=0.01$; ---, $x_0/\lambda=0.05$; ——, $x_0/\lambda=0.15$; — - —, $x_0/\lambda=0.20$; ○, $x_0/\lambda 0.25$; *, $x_0/\lambda=0.33$; ×, $x_0/\lambda=0.40$; +, $x_0/\lambda=0.48$. The separatrix shown as a solid line: (a) $T=2.8$; (b) $T=6.4$; (c) $T=5.7$; (d) $T=7.1$.

Particle ejection and separatrix crossing for $St=10$ and 100 are also shown in Fig. 5. These particles exhibit a stronger dependence of cross-stream displacement on initial position than observed for $St=1$ as well as a trend towards maximum lateral transport corresponding to initial positions shifting towards the core. Note that for $St=10$, most of the particles are ejected into the freestream within the time interval shown ($0 \leqslant T \leqslant 5.7$) and acquire somewhat parallel trajectories. The strong time dependence of the transport is also clear, i.e., the lateral transport for $St=10$ and $x_0/\lambda=0.25$ is in fact larger than for $St=1$ within about six vortex turnover times. It appears from Fig. 5 that for increasing particle inertia (i.e., larger St), particles cross the separatrix at larger angles. This implies that the transverse particle velocity increases relative to the horizontal component. This is consistent with the fact that particle residence times in the vortex core region increase with increasing inertia. The transverse fluid velocity that develops as the layer rolls up cumulatively induces a larger vertical particle velocity for large-inertia particles. Thus, a larger alteration of cross-stream displacement for $St=10$ and 100 using nonuniform seeding occurs at later times than is possible for $St=1$. For $St=1$ the initial conditions are less dominant with particles being transported to the periphery of the vortex. This in turn nearly eliminates the influence of nonuniform seeding on dispersion.

The results in Fig. 5, as well as for longer time intervals than shown in the figure, can be used to determine the optimal seeding location in the distribution (12). In particular, the peak in (12) for fluid elements and $St=1$, 10, and 100 to be used in subsequent calculations of mean-square dispersion

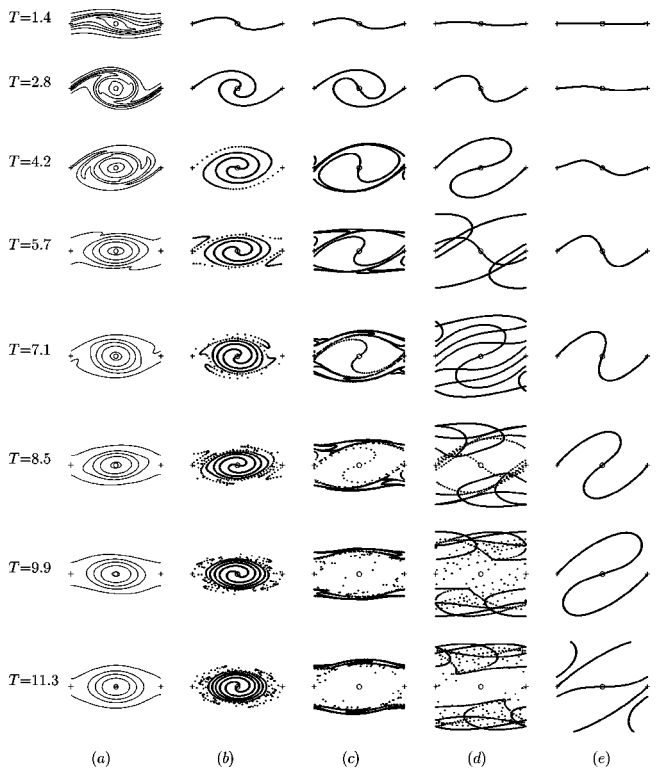

FIG. 6. Vorticity contours and particle distributions from initial seedings along the layer interface. +, saddle points; ○, vortex center. (a) vorticity; (b) $St=0.05$; (c) $St=1$; (d) $St=10$; (e) $St=100$.

will be $x_0/\lambda = 0$, 0, 0.2 and 0.25, respectively. At sufficiently long times, nonuniform seedings with this peak location should yield larger dispersion compared to a uniform initial distribution, with the exception of $St=1$.

2. Vorticity field and particle distributions

Temporal development of the fluid vorticity field and particle distributions are useful for providing insight into the effect of nonuniform seeding and also illustrate the additional mechanisms relevant to finite-inertia particles discussed in the Introduction. Vorticity contours and particle distributions for each Stokes number are shown in Fig. 6. Fig. 6(a) shows the formation of a large scale spanwise vortex, with a well-defined roller developed by $T=2.8$. Note that there is no subharmonic perturbation and therefore vortex pairing is prohibited. The ''wobbling'' (vortex nutation) evident in the particle trajectories (cf. Fig. 5) is also clear in Fig. 6(a). The corresponding particle distributions are shown in Figs. 6(b)–6(e) for $St=0.05$, 1, 10, and 100, respectively (note that only the locations of every tenth particle have been shown in the figures). The particles appear to form continuous curves at early times in the evolution whereas individual particles are identifiable at later times. As expected, distributions for $St=0.05$ in Fig. 6(b) are quite similar to fluid elements. These particles are able to follow the flow relatively well and near the core region of the vortex the distribution becomes more spiral-like with increasing time. The distribution near the vortex edge is more complicated with many 'lobes' appearing at later times. Though not obvious from the figure, some particles cross the separatrix and are then re-entrained back to the core region.

Prior to $T=2.8$ the distribution for $St=1$ shown in Fig. 6(c) is similar to that for $St=0.05$. At later times, however, the distribution becomes very different due to the inability of the particles to follow the flow. Particles are efficiently transported from the core region, e.g., at $T=9.9$ the core region appears to be devoid of particles. More importantly, by $T=9.9$ most particles are concentrated in regions not far from the edge of the vortex, consistent with the relative insensitivity to initial position shown in Fig. 5. For $St=10$ and 100, particles are also transported from the core region (Figs. 6(d)–6(e)). The figure also shows that particles with larger St require more time to travel from the interface, consistent with their greater response time. This dependence of dispersion on both time and Stokes number is quite consistent with several previous studies (e.g., Samimy and Lele,[8] and Wen *et al.*[10]).

3. Development of cross-stream displacement

A useful measure of the time-dependence of lateral dispersion is the temporal development of the particle cross-stream displacement as a function of the initial streamwise location. This quantity is shown in Fig. 7 for $St=0.05$, 1, 10, and 100. Because of symmetry, only the left half of the layer is shown. The results shown in the figure correspond to later times in the evolution of the flow after which the layer is well developed and most particles have crossed the separatrix (cf. Figs. 5–6). Figure 7(a) for $St=0.05$ is similar to that obtained for fluid elements obtained by Wang[16] and shows that with increasing time the streamwise location corresponding to maximum lateral transport moves towards the saddle, similar to the behavior observed for the Stuart vortex (cf. Fig. 1(c)). As the layer rolls up, resulting in the spiral-like distributions shown in Fig. 6(b), the curves in Fig. 7(a) oscillate about the interface, the oscillation being caused by particles initially near the saddle being transported to the outer region of the layer and subsequently circulating about the core while particles near the core follow circulatory motions about the center.

As can also be observed, the additional mechanisms affecting finite-inertia particle transport result in very different behavior as the Stokes number is increased. The behavior for $St=1$ is again interesting, with the ''asymptotic'' transport being $y/\lambda \approx \pm 0.25$, independent of the initial seeding. The apparent discontinuities near $x_0/\lambda = 0.1$ and 0.35 in Fig. 7(b) occurring because particles initially close together can be far apart at long times. It is also interesting to note that, though Fig. 7(b) again shows that nonuniform seeding will not be an effective approach for increasing lateral transport for $St=1$, it does suggest the possibility of controlling the transport into the positive (or negative) cross-stream direction. For example, particles will be transported to the upper part of the layer if they are initially seeded at streamwise locations $x_0/\lambda < 0.1$ and to the lower part if the initial distribution is $0.1 < x_0/\lambda < 0.35$. Note that this feature for $St=1$ is not dependent on time while Fig. 7(a) shows that control of the

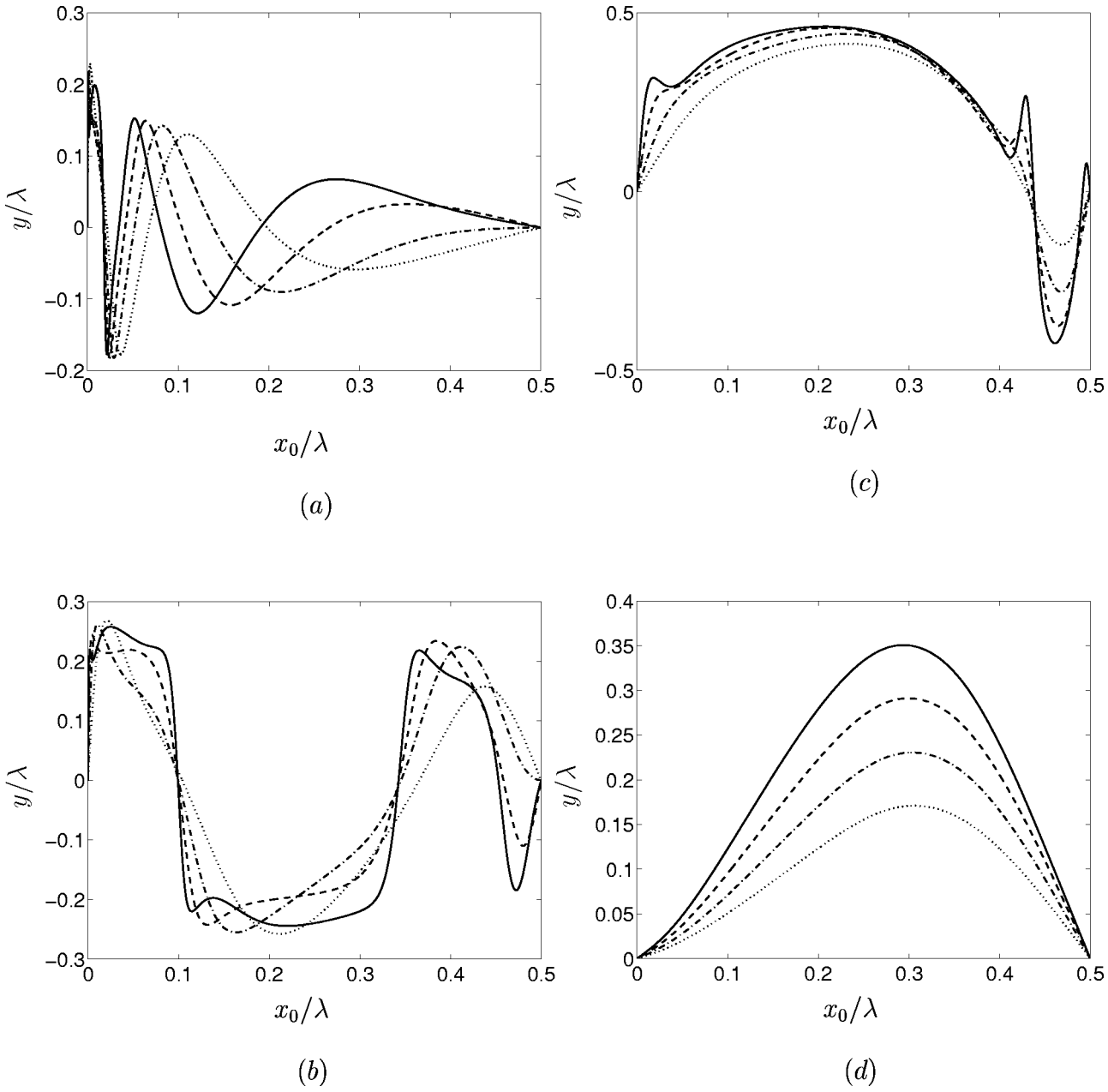

FIG. 7. Particle cross-stream position as a function of initial streamwise location x_0. (a) $St=0.05$: ···, $T=4.7$; — · —, $T=5.1$; ---, $T=5.5$; ——, $T=5.9$. (b) $St=1$: ···, $T=4.2$; — · —, $T=4.8$; ---, $T=5.4$; ——, $T=5.9$. (c) $St=10$:···, $T=5.7$; — · —, $T=6.5$; ---, $T=7.4$; ——, $T=8.2$. (d) $St=100$: ···, $T=5.7$; –·–, $T=6.5$; ---, $T=7.4$; ——, $T=8.2$.

cross-stream displacement for $St=0.05$ is strongly dependent on the time interval of interest.

For $St=10$ and 100 the temporal development shown in Figs. 7(c) and 7(d) is consistent with the trajectories in Fig. 5. With increasing response time the curves develop more slowly with fewer oscillations than for the smaller Stokes numbers, i.e., the particles are less able to follow the curved trajectories of the fluid. For $x_0/\lambda=0.4-0.5$ the curves develop a discontinuity with increasing time as particles close to the core cross the lower separatrix. A comparison of Figs. 7(c) and 7(d) also shows the peak in the displacement shifting towards the core as St increases, further consistent with the trajectories in Fig. 5.

4. Mean-square dispersion

Particle mean-square dispersion in the cross-stream direction for initial seedings of varying nonuniformity is shown in Fig. 8. The initial distribution corresponding to $\sigma=0.5$ is nearly the same as a uniform distribution while smaller σ corresponds to increasingly nonuniform seedings (i.e., more particles initially near $x_0=x_m$). In the initial stages of the evolution (within 2–3 turnover times) a more uniform distribution (larger σ) results in larger Y^2 for $St=0.05$ (Fig. 8(a)). This is consistent with Fig. 7(a) which shows the initial location corresponding to the largest displacement is initially away from the saddle point. With in-

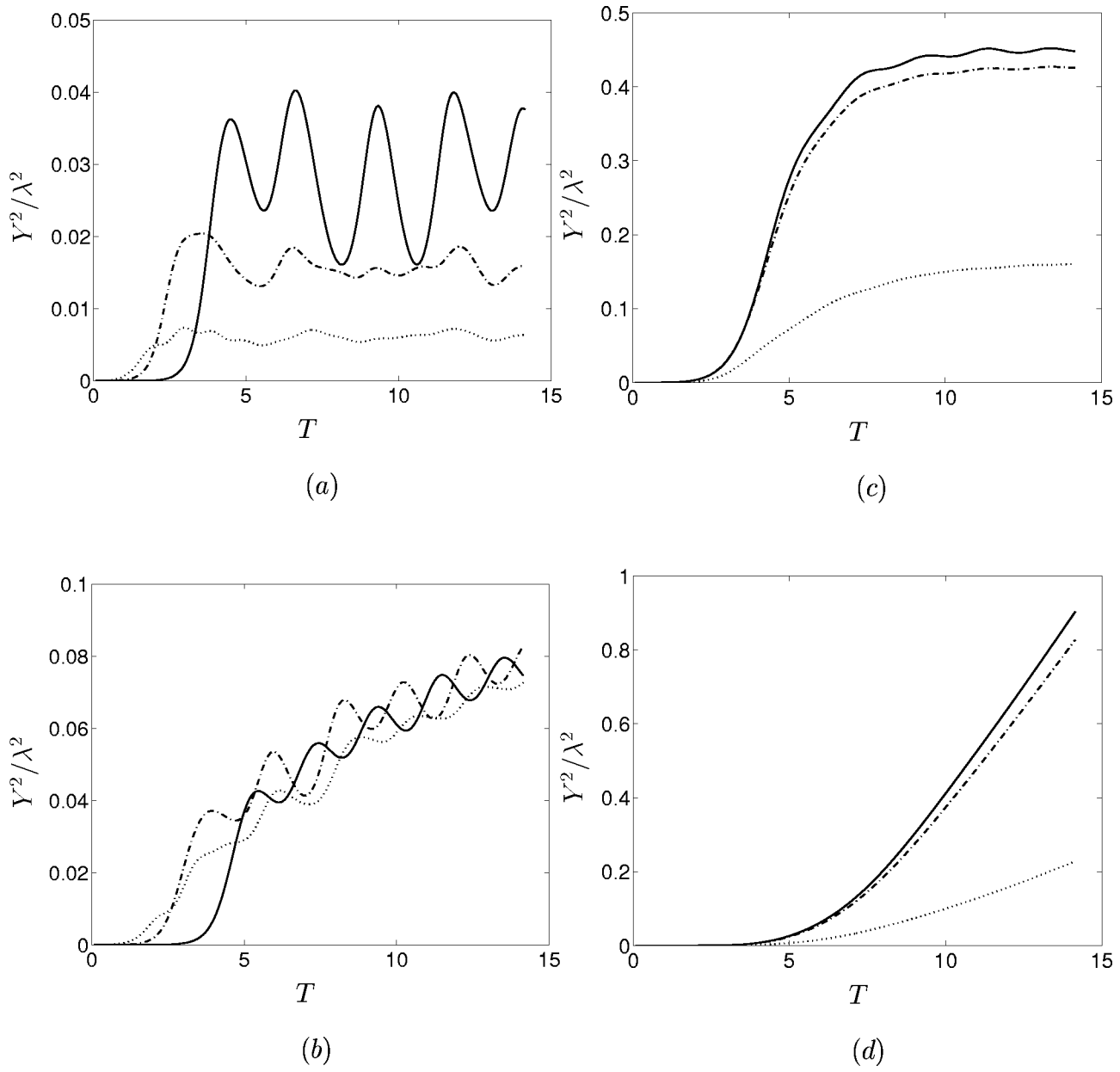

FIG. 8. Mean-square dispersion in the cross-stream direction for interface seeding. (a) $St=0.05$, $x_m/\lambda=0$; (b) $St=1$, $x_m/\lambda=0$; (c) $St=10$, $x_m/\lambda=0.2$; (d) $St=100$, $x_m/\lambda=0.25$, $\cdots$, $\sigma=0.5$; — - —, $\sigma=0.05$; ——, $\sigma=0.005$.

creasing time the greater lateral extent of streamlines near the saddle point becomes important and nonuniform seedings with a large fraction of light particles near the saddle have the greatest lateral transport. At $T\approx 12$, for example, the mean-square dispersion for $\sigma=0.005$ is about 5–6 times larger than that resulting from a uniform distribution. It is also clear from the figure that the curves corresponding to small σ develop oscillations in response to the quasi-periodic shrinking and expansion of the vortex.

While the dispersion for $St=0.05$ is similar to that of fluid elements discussed in Wang,[16] the dispersion of particles with larger Stokes numbers are quite different. The oscillatory behavior in Y^2 is reduced by increasing inertia since the particles do not follow the fluid, are ejected from the core region, and cross the separatrix into the freestream. Figure 8(b) is again consistent with the fact that the dispersion for $St=1$ is insensitive to nonuniform seeding. Conversely, for particles with larger inertia, Figs. 8(c) and 8(d) show that large increases in lateral transport can be achieved by seeding more particles near $x_0/\lambda=0.2$ and $x_0/\lambda=0.25$ for $St=10$ and $St=100$, respectively.

It should again be remarked that Fig. 8 demonstrates the complicated effect of the mechanisms described in the Introduction on the transport of finite-inertia particles. The transverse dispersion of fluid elements and light particles can be maximized for nonuniform seedings with a peak near the saddle points, though this process is clearly time-dependent, as Fig. 8(a) shows, with increases in lateral transport being achieved after about $3-4(\lambda/\Delta U)$ for $St=0.05$. For increasing particle inertia, vortex ejection and subsequent separatrix crossing shifts the peak towards the center of the vortex. However, for Stokes numbers of order unity there is an effi-

cient transport of particles to the outer region of the vortex (near the separatrices) with little sensitivity of lateral transport to initial seeding. With further increases in response time ($St=10$ and 100), transport becomes increasingly sensitive to its previous motion with ejection from the core region and separatrix crossing into the freestream leading to large increases in dispersion for nonuniform seedings. Within $5(\lambda/\Delta U)$ the mean-square dispersion for $St=10$ is in fact larger than for $St=1$ and by $10(\lambda/\Delta U)$ particles with $St=100$ exhibit the largest lateral transport. Thus, in addition to a sensitivity to the initial location, lateral dispersion is also time- and Stokes-number dependent.

B. Off-interface seeding

In the previous section the dispersion of particles initially seeded along the interface was considered. In applications, particles can be seeded at various locations (simultaneously) along the cross-stream direction. Seeding away from the interface is investigated in this section in order to gain further insight into the effect of nonuniform seeding on dispersion. In particular, a line seeding at $y_0/\lambda=0.1$ is examined, which is within the vortex core region for $0.22<x_0/\lambda<0.78$, in the context of the Stuart vortex (cf. Fig. 1(a)). For the evolving mixing layer the vortex core size increases with time, and $y/\lambda=0.1$ is representative of the intermediate location where both the freestream and the roll up of the vortex affect subsequent dispersion. For larger cross-stream positions particles travel predominantly in the streamwise direction while for smaller cross-stream locations the dispersion will be similar to that observed in the previous section for interface seeding. This off-interface release of particles, along with the interface release discussed in the last section, can be viewed as building blocks of the more general particle injection, such as multiple-line injection or half layer injection. The assumption that particle motion does not modify the fluid flow implies that any general injection can be analyzed as a superposition of line injections.

1. Particle trajectories

Similar to the procedure described in Sec. IV A, particle trajectories for fluid elements and $St=1$, 10, 100 were computed for the off-interface release. Particle velocities were initially equal to that of the fluid at the particle position. For large St, this initial condition complicates comparison of results from this section to those from Sec. IV A for an interface seeding in which the initial particle velocity was zero. For smaller inertia, however, the effect of the initial particle velocity is less significant. Figure 9 shows trajectories for particles initially at $y_0/\lambda=0.1$ and $0<x_0/\lambda<0.5$. Unlike the interface seeding where the transport of fluid elements initially near $x_0/\lambda=0.5$ is in the core region, fluid particles seeded at $y_0/\lambda=0.1$ are transported to the outer region of the vortex regardless of their initial streamwise location. The figure also shows that some trajectories cross the separatrix and are subsequently re-entrained into the core region. In addition, the lateral transport of fluid elements initially near $x_0=0$ is larger than those seeded near the center of the domain, indicating that nonuniform seeding with the largest fraction of particles near $x_0=0$ can enhance dispersion. However, since the lateral extent of streamlines emanating from $x_0=0$ compared to other streamwise positions is not as large compared to the interface release, the increase in transport is smaller than observed in Sec. IV A.

Particle trajectories for $St=1$ from initial locations $0<x_0/\lambda<0.5$ are shown in Fig. 9(b). Similar to the behavior observed for the interface seeding in Sec. IV A (cf. Fig. 5), for an initial cross-stream seeding at $y_0/\lambda=0.1$, most of the trajectories asymptote towards $y/\lambda\approx0.25$ at long times, independent of the initial streamwise location, and again implying a weak dependence of lateral dispersion on nonuniform seeding. For $St=10$ and 100 (Figs. 9(c), 9(d)), the trajectories for long times are shown. Unlike the behavior observed for $St=1$ and similar to that observed for the interface seeding (cf. Fig. 5), the figure shows a sensitivity of lateral displacement to initial position with particle motion becoming nearly parallel to the freestream at long times. The streamwise position corresponding to the maximum displacement occurs at approximately $x_0/\lambda=0.40$ and 0.48 for $St=10$ and 100, respectively.

Trajectories from initial positions $0.5<x_0/\lambda<1$ are similar except that more particles are ejected into the lower freestream. Calculations of mean-square dispersion presented in the subsequent figures are performed with peak values of the initial seeding determined from Figs. 9 and similar trajectories with initial seedings $0.5<x_0/\lambda<1$. In particular, the peaks are $x_{m1}=x_{m2}=0$ for $St=0.05$, $x_{m1}=x_{m2}=0$ for $St=1$, $x_{m1}=0.4$ and $x_{m2}=0.48$ for $St=10$, and $x_{m1}=x_{m2}=0.48$ for $St=100$. Dispersion for the nonuniformly seeded distributions should be larger than that for a uniform seeding, with the exception of $St=1$ in which the dispersion is again observed to become independent of initial position.

2. Mean-square dispersion

Cross-stream dispersion, Y^2, for different initial seedings from $y_0/\lambda=0.1$ is shown in Fig. 10. As expected, the nonuniform distributions yield larger dispersion than obtained for a uniform seeding, with the exception of $St=1$ where cross-stream dispersion is relatively independent of initial position. Consistent with the particle trajectories shown earlier, Fig. 10 shows that there are smaller increases in cross-stream dispersion using nonuniform seedings for the off-interface release as compared to the interface seeding considered in Sec. IV A (cf. Fig. 8). In addition, the cross-stream dispersion for the off-interface release is also smaller than previously obtained for the interface seedings. This general feature is expected since both the local fluid transverse velocity and ejection due to fluid vorticity are reduced at locations away from the interface.

V. SUMMARY

Previous examinations have shown that fluid element dispersion can be enhanced by nonuniform seeding with a greater fraction of particles near the saddle point (Wang[16]). In general, particle ejection from vortex cores, separatrix crossing, and the effect of initial velocities shift the optimal

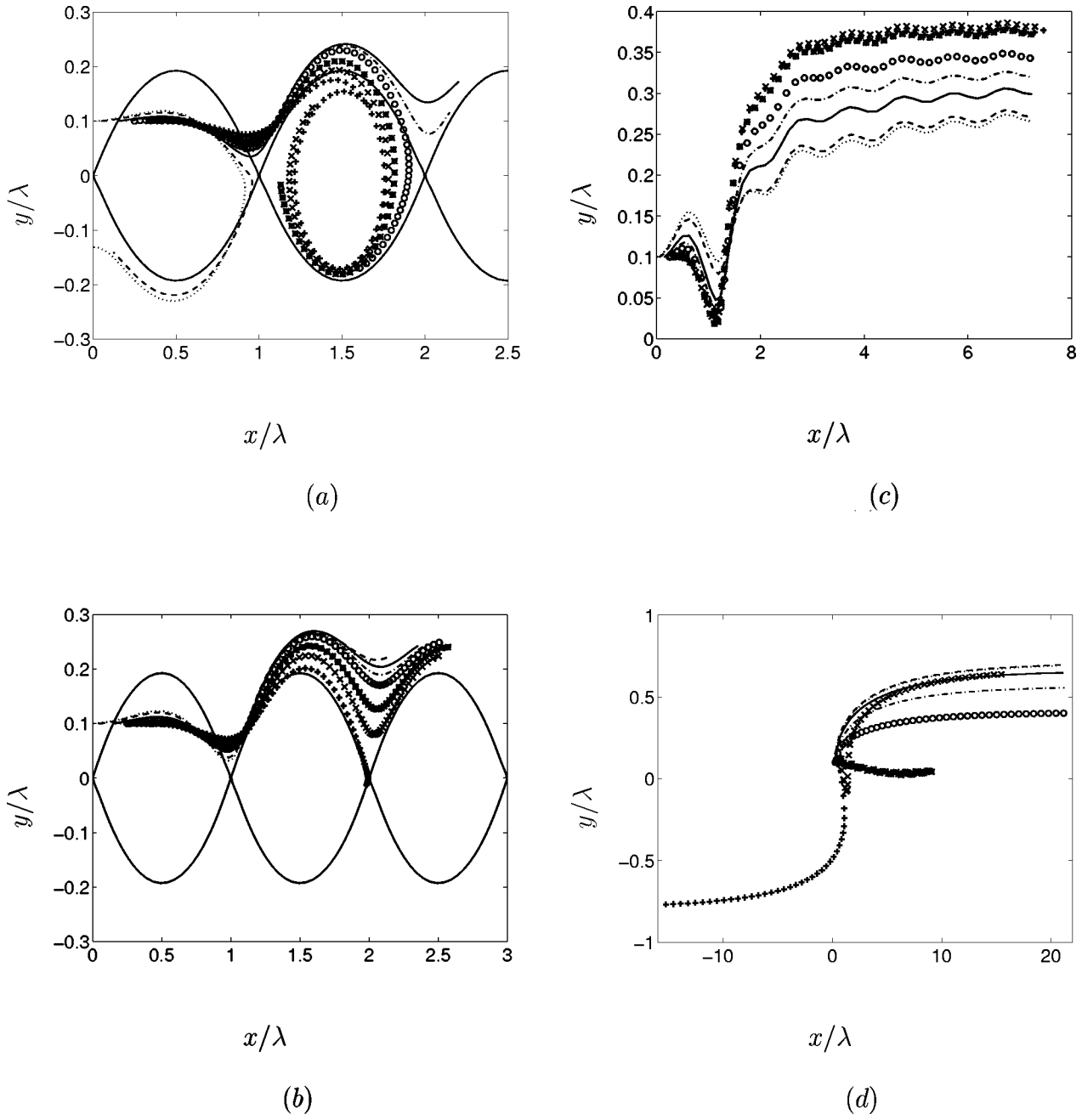

FIG. 9. Particle trajectories from initial locations $y_0/\lambda=0.1$ and $0<x_0/\lambda<0.5$. (a) Fluid elements, $0\leqslant T\leqslant 5.7$; (b) $St=1$, $0\leqslant T\leqslant 5.7$; (c) $St=10$, $0\leqslant T\leqslant 17.0$; (d) $St=100$, $0\leqslant T\leqslant 56.6$. Initial streamwise location: $\cdots$, $x_0/\lambda=0.01$; ---, $x_0/\lambda=0.05$; ——, $x_0/\lambda 0.15$; — - —, $x_0/\lambda=0.20$; ○, $x_0/\lambda=0.25$; ∗, $x_0/\lambda=0.33$; ×, $x_0/\lambda=0.40$; +, $x_0/\lambda=0.48$. The separatrix at $T=5.7$ is also shown with solid lines (——) in (a) and (b).

seeding location of finite-inertia particles towards the vortex core. Nonuniformly seeded finite-inertia particles exhibit substantial increases in dispersion compared to uniform initial distributions. For Stokes numbers of order unity it is very interesting to note, however, that particles are ejected from the core region and dispersion at long times is nearly independent on initial position.

In general, the optimal seeding maximizing dispersion is dependent upon both the time interval of interest and Stokes number. This is particularly relevant to temporally and/or spatially developing flows. For example, previous studies have shown that particles with response times comparable to the time-scale of the large-scale structures in free shear flows, i.e., $St=1$, can have greater dispersion than fluid elements (e.g., see Samimy and Lele,[8] Wen *et al.*,[10] and Crowe *et al.*[13–15]). The enhanced dispersion for $St=1$ is also observed in the present study, though it should be noted that the effective Stokes number corresponding to maximum dispersion is time dependent. Initially, particles with small Stokes numbers have the largest dispersion while at long times particles with large Stokes numbers have sufficient time to respond to the flow and can also exhibit large dispersion (e.g., see Figs. 8 and 10). For intermediate evolution times particles with $St\approx 1$ have the greatest dispersion compared to

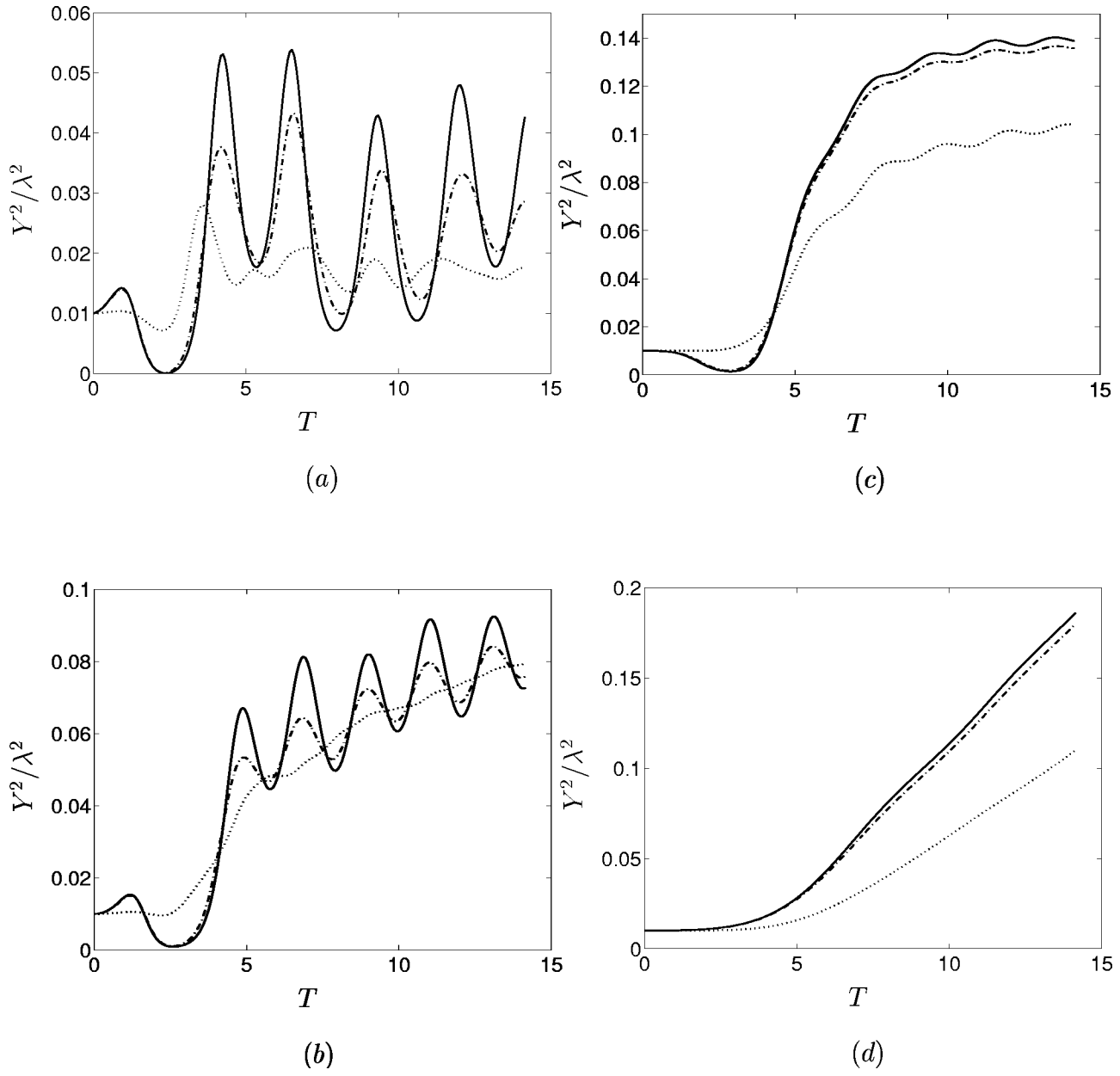

FIG. 10. Mean-square dispersion in the cross-stream direction for off-interface seeding. (a) $St=0.05$, $x_{m1}/\lambda=x_{m2}/\lambda=0$; (b) $St=1$, $x_{m1}/\lambda=x_{m2}/\lambda=0$; (c) $St=10$, $x_{m1}/\lambda=0.4$, $x_{m2}/\lambda=0.48$; (d) $St=100$, $x_{m1}/\lambda=x_{m2}/\lambda=0.48$. $\cdots$, $\sigma=0.5$; — · —, $\sigma=0.05$; ——, $\sigma=0.005$.

both smaller and larger Stokes numbers. This is due to the definition of St which is based on the initial flow time scale, while the time scale based on vorticity thickness increases as the mixing layer thickness grows and thus the effective Stokes number for a given response time decreases with time.

The effect of nonuniform seeding was also studied for a cross-stream position away from the interface where both the freestream flow and vortex roll up affect dispersion. The purpose was to gain some insight into applications in which particles are seeded across an entire stream of the flow. Nonuniform seeding is also effective for off-interface seedings, though the increase in dispersion is not as large compared to nonuniform seedings along the interface. Similar to interface seedings, the dispersion for $St=1$ at long times is not enhanced since these particles are efficiently transported to the outer region of the vortex, independent of their initial location.

The present work focused on relatively simple fluid flows which are two-dimensional and in which there was no vortex pairing. Nevertheless, particle motion in both the Stuart vortex and unsteady mixing layer is complex and very difficult to predict. In three-dimensional flows with vortex pairing and small-scale turbulence the parameter space relevant to dispersion enhancement using nonuniform seeding will increase. In addition, different vortical structures may arise in three-dimensional flows which could alter the types of nonuniform seedings used to maximize dispersion. The reader is referred to Marcu and Meiburg[29] and Tong and Wang[30] for a recent examination of particle dispersion in three-dimensional mixing layers.

ACKNOWLEDGMENTS

This work is supported by the National Institute of Occupational Safety and Health (Grant Number OH03052-03). Computer time for the simulations was supplied by the Cornell Theory Center.

[1]G. L. Brown and A. Roshko, ''On density effect and large structure in turbulent mixing layers,'' J. Fluid Mech. **64**, 775 (1974).
[2]C. D. Winant and F. K. Browand, ''Vortex pairing, the mechanism of turbulent mixing layer growth at moderate Reynolds number,'' J. Fluid Mech. **63**, 237 (1974).
[3]C.-M Ho and P. Huerre, ''Perturbed free shear layers,'' Annu. Rev. Fluid Mech. **16**, 365 (1984).
[4]B. J. Lazaro and J. C. Lasheras, ''Particle dispersion in the developing free shear layer. Part 1. Unforced flow,'' J. Fluid Mech. **235**, 143 (1992a).
[5]B. J. Lazaro and J. C. Lasheras, ''Particle dispersion in the developing free shear layer. Part 2. Forced flows,'' J. Fluid Mech. **235**, 179 (1992b).
[6]C. T. Crowe, R. A. Gore, and T. R. Trout, ''Particle dispersion by coherent structures in free shear flows,'' Part. Sci. Technol. **3**, 149 (1985).
[7]R. Chein and J. N. Chung, ''Effects of vortex pairing on particle dispersion in turbulent shear flows,'' Int. J. Multiphase Flow **13**, 785 (1987).
[8]M. Samimy and S. K. Lele, ''Motion of particles with inertia in a compressible free shear layer,'' Phys. Fluids A **3**, 1915 (1991).
[9]K. Hishida, A. Ando, and M. Maeda, ''Experiments on particle dispersion in a turbulent mixing layer,'' Int. J. Multiphase Flow **18**, 181 (1992).
[10]F. Wen, N. Kamalu, J. N. Chung, C. T. Crowe, and T. R. Troutt, ''Particle dispersion by vortex structures in plane mixing layers,'' J. Fluids Eng. **114**, 657 (1992).
[11]J. E. Martin and E. Meiburg, ''The accumulation and dispersion of heavy particles in forced two-dimensional mixing layer. I. The fundamental and subharmonic cases,'' Phys. Fluids **6**, 1116 (1994).
[12]N. Raju and E. Meiburg, ''The accumulation and dispersion of heavy particles in forced two-dimensional mixing layer. Part 2: The effect of gravity,'' Phys. Fluids **7**, 1241 (1995).
[13]C. T. Crowe, J. N. Chung, and T. R. Troutt, ''Particle mixing in free shear flows,'' Prog. Energy Combust. Sci. **14**, 171 (1988).
[14]C. T. Crowe, J. N. Chung, and T. R. Troutt, ''Particle dispersion by organized turbulent structures,'' in *Particulate Two-Phase Flow*, edited by M. C. Roco (Butterworth-Heinemann, Boston, 1993), p. 627.
[15]C. T. Crowe, J. N. Chung, and T. R. Troutt, ''Numerical models for two-phase turbulent flows,'' Annu. Rev. Fluid Mech. **28**, 11 (1996).
[16]L.-P. Wang, ''Dispersion of particles injected nonuniformly in a mixing layer,'' Phys. Fluids A **4**, 1599 (1992).
[17]M. R. Maxey, ''The gravitational settling of aerosol particles in homogeneous turbulence and random flow fields,'' J. Fluid Mech. **174**, 441 (1987).
[18]L.-P. Wang and M. R. Maxey, ''Kinematical descriptions for mixing in stratified or homogeneous shear flows,'' in *Mixing in Geophysical Flows—Effects of Body Forces in Turbulent Flows*, edited by J. M. Redondo and O. Metais, Universitat Politecnica de Catalunya, Barcelona, December 1992 (Kluwer, Dordrecht, 1993).
[19]J. T. Stuart, ''On finite amplitude oscillations in laminar mixing layers,'' J. Fluid Mech. **29**, 417 (1967).
[20]E. Meiburg and P. K. Newton, ''Particle dynamics and mixing in a viscosity decaying shear layer,'' J. Fluid Mech. **227**, 211 (1991).
[21]M. R. Maxey and J. J. Riley, ''Equation of motion for a small rigid sphere in a nonuniform flow,'' Phys. Fluids **26**, 883 (1983).
[22]J. Kim and P. Moin, ''Application of a fractional-step method to incompressible Navier–Stokes equations,'' J. Comput. Phys. **59**, 308 (1985).
[23]J. B. Perot ''An analysis of the fractional step method,'' J. Comput. Phys. **108**, 51 (1993).
[24]X. Wu, K. D. Squires, and Q. Wang, ''On extension of the fractional step method to general curvilinear coordinate systems,'' Numer. Heat Transfer, Part B **27**, 175 (1994).
[25]G. P. Williams, ''Numerical integration of the three-dimensional Navier–Stokes equations for incompressible flow,'' J. Fluid Mech. **37**, 727 (1969).
[26]A. Michalke, ''On the inviscid instability of the hyperbolic-tangent velocity profile,'' J. Fluid Mech. **19**, 543 (1964).
[27]Q. Wang, K. D. Squires, and X. Wu, ''Lagrangian statistics in turbulent channel flow,'' Atmos. Environ. **29**, 2417 (1994).
[28]S. K. Aggarwal, ''Relationship between Stokes number and intrinsic frequencies in particle-laded flows,'' AIAA J. **32**, 1323 (1994).
[29]J. E. Marcu and E. Meiburg, ''Three-dimensional features of particles dispersion in a nominally plane mixing layer,'' Phys. Fluids **8**, 2266 (1996).
[30]X.-L. Tong and L.-P. Wang, ''Direct simulations of particle transport in two and three dimensional mixing layer,'' in *ASME Gas–Solid Flows*, ASME Fluids Engineering Division Summer Meeting, Vancouver, British Columbia, 1997.